Cellular Guardband NB-IoT Performance Over PMMA Plastic Optical Fibers

M. Waseem, A. López, P. L. Carro, *Fellow, IEEE*, and M. A. Losada

***Abstract*—Over the last decade, the growing demand of connectivity has produced a rapid evolution of 5G technology to answer the requirements of relevant areas such as Internet of Things (IoT). Radio and optical technology convergence appears as a solution to fulfill the needs of the future networks, exploiting the high bandwidth-range of optical fibers with the ubiquity and mobility of radio communications. The concept of Radio-over-Fiber has usually been applied successfully using silica fibers to transmit light from a modulated laser to a photodetector for demanding applications. In this work, we propose to evaluate the performance of Polymer Optical Fiber (POF) links to carry RF signals for those applications where their limited bandwidth-length product is sufficient, while their fast and cost-effective deployment is paramount. In particular, we analyze the performance of the downlink transmission of Long Term Evolution (LTE) and guardband Narrow-Band Internet of Things (NB-IoT) signals through a 75-m Poly(methyl methacrylate) – PMMA Graded-Index POF. Our study considers a comprehensive set of LTE carrier frequencies and bandwidths.**

***Index Terms*—Internet of Things (IoT), long term evolution (LTE), optical communications, plastic optical fibers, radio over fiber (RoF), radio over pof (RoPOF).**

I. Introduction

RADIO-over-fiber (RoF) is a well established technology initially devised to address the issue of spectral congestion in the lower microwave region providing a backbone network with wireless and wired connectivity. In this context, RoF takes advantage of the wide bandwidth of optical fibers to transmit broadband radiofrequency (RF) signals up to extended distances [1]. Recently, the evolution of the 5G and beyond mobile network has shifted the application of RoF technology to the design of efficient architectures for mobile fronthaul systems needed to cope with the optical bottleneck [2]. The higher capacity requirements of the new generation cellular networks have been motivated by the increasing number of mobile devices with internet applications that consume an enormous volume of data. In addition, new paradigms like Internet of Things (IoT) networking, demand a massive number of connections to heterogeneous devices [3]. In this context, The 3rd Generation Partnership Project (3GPP) introduced a narrowband wide area cellular system (named NB-IoT) to provide low power and low cost connectivity for IoT devices, basing its implementation on existing features of Long Term Evolution (LTE) [4], [5].

The majority of proposed RoF systems and techniques rely on Glass Optical Fibers (GOFs), mainly standard Single Mode Fibers (SMF), which take advantage of the extensive deployments in metro Wavelength-Division-Multiplexing (WDM) and access Passive Optical Networks (PONs) [6], [7]. However, Multi-Mode glass Fibers (MMF) and polymer optical fibers have also been used for short range applications [8], [9], [10], [11], [12].

The term Polymer or Plastic Optical fiber (POF) is assigned to all kinds of optical fibers whose core and cladding are manufactured from polymeric compounds such as Poly(methyl methacrylate) (PMMA) and deuterated or perfluorinated polymers [13]. Generally, the standard POFs are manufactured from PMMA, which has an attenuation 1000 times higher than Silica glass (90–200 dB/km), with several minima in the visible region (520–670 nm). Standard POFs have relatively large core diameters (around 1 mm) and high numerical apertures (0.3 to 0.6) which, together with their step-index (SI) profiles, are the cause of their large modal dispersion. There are also polymer fibers with Graded-Index (GI) profiles that exhibit lower modal dispersion. In fact, the GI-POFs made of perfluorinated materials (PF GI-POFs) have attenuation and dispersion comparable to those of MMFs [14]. The former can easily support transmission rates higher than 10 Gb/s for hundreds of meters using infrared sources, thus providing a direct replacement of multimode GOFs for high performance networks [15]. However, perfluorinated GI-POFs have smaller sizes and apertures than standard POFs, losing some of their advantages. On the other hand, there are few commercially available models of PMMA GI-POF, which have demonstrated a performance superior to SI-POFs. Their performance is still below that of the PF GI-POFs but their larger cores and numerical apertures preserve some of the advantages of the PMMA SI-POFs [16]. These PMMA GI-POFs have a relatively flat frequency response, but their higher attenuation reduce the transmission rate to less than 2 Gb/s at distances above 50 meters [17].

The moderate bandwidth-length products of PMMA SI-POFs have not posed an obstacle to their use in scenarios where their robustness, manipulability and cost-effectiveness are key features. In fact, large-core SI-POFs are well established in the automotive industry and the standard MOST (Media oriented

Manuscript received 31 March 2023; revised 9 September 2023 and 6 October 2023; accepted 31 October 2023. Date of publication 9 November 2023; date of current version 2 December 2023. This work was supported in part by the Spanish Ministry of Science and Innovation (MICINN/FEDER), under Grant PID2021-122505OB-C33, and in part by the DGA, under Grants T20-23R and T31-23R. *(Corresponding author: A. López.)*

The authors are with the Aragón Institute of Engineering Research (i3A), Universidad de Zaragoza, 50018 Zaragoza, Spain (e-mail: 806405@unizar.es; aliclope@unizar.es; plcarro@unizar.es; alosada@unizar.es).

Color versions of one or more figures in this article are available at https://doi.org/10.1109/JLT.2023.3331328.

Digital Object Identifier 10.1109/JLT.2023.3331328

© 2023 The Authors. This work is licensed under a Creative Commons Attribution 4.0 License. For more information, see https://creativecommons.org/licenses/by/4.0/

Systems Transport) is now installed inside millions of vehicles [18]. In addition, POFs are widely used to implement industrial control networks and factory automation to provide reliable communication lines in harsh industrial manufacturing environments [19]. Moreover, their ease of handling that leads to lower installation and maintenance costs was decisive to introduce them into domestic scenarios [20], [21], [22]. Although automotive and industrial standards are limited to data rates of 150 Mb/s and distances up to 50 meters, advanced modulation formats that increase the spectral efficiency of POF systems have been investigated [23]. Today, several companies offer connectivity at 1 Gb/s for in-home networks through a combination of a SI-POF backbone with room Wi-Fi access points [24] demonstrating that the convergence of radio and optical technologies is a good approach in domestic scenarios. Indeed, it is in the context of in-building and in-home networks where research on Radio over POF (RoPOF) technologies has been concentrated, showing the viability to carry multi-format signals using per-fluorinated POFs [12], [25], and PMMA POFs [26], [27], [28]. It is precisely the on-going deployment of IoT in the smart homes to achieve home automation and remote control management what has raised the demand of network capacity and connectivity [29]. These needs are shared by the automotive business to advance the development of autonomous and safe vehicles [30], and by the achievement of Industrial IoT (IIoT) [31].

In this work, we aim at analyzing the prospects of PMMA POF links in future hybrid fiber-wireless networks. For this purpose, we have implemented the downlink joint transmission of Long Term Evolution (LTE) and guardband NB-IoT signals through a 75-m PMMA GI-POF, using off-the-shelf transmitters and receivers. In a previous work we have reported the first results for a carrier frequency of 800 MHz and 10-MHz LTE bandwidth [32]. Here, we extend this study to other carrier frequencies and bandwidths. We analyze three LTE carrier frequencies: 460 MHz, 800 MHz and 1800 MHz and quantify the effect of different parameters such as LTE bandwidth, RF input power and relative power level between signals, over the transmission performance in terms of Error Vector Magnitude (EVM). The paper is organized as follows: In Section II, the experimental setup, the signals and the transmission parameters are described. In Section III, the experimental results are presented, analyzed, and discussed. Finally, we summarize the conclusions obtained with our research in Section IV.

II. LTE + NB-IoT Signal Transmission Over GI-POF

The study was experimentally carried out by transmitting over the large-core POF the downlink RF signals formatted according to 64-QAM and QPSK schemes for the LTE and NB-IoT, respectively. For this purpose, a RoPOF communications link was built by using commercial off-the-shelf electronic and optical components. The digital signal processing tasks as signal generation, demodulation and EVM estimation were performed offline using a computer.

A. Experimental Set-Up

The experimental set-up used for the measurements is represented in Fig. 1. The LTE and NB-IoT downlink signals

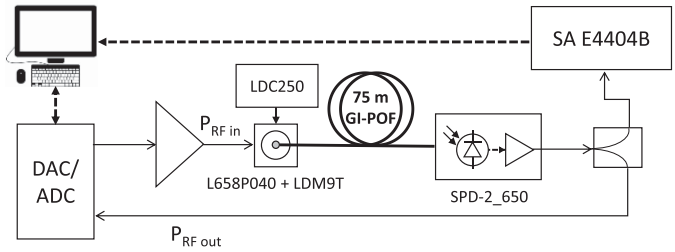

Fig. 1. Experimental set-up.

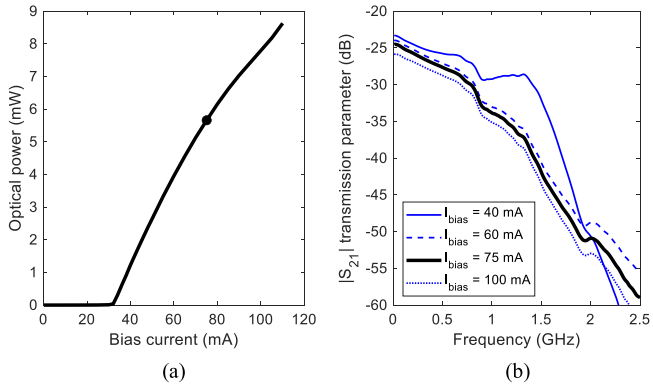

Fig. 2. Back-to-back measurements using a 75-cm GI-POF pigtail: power characteristic curve of the transmitter (a) and normalized system frequency response (b).

were computer-generated and combined using software based on the LTE toolbox of MATLAB. This combined signal was then delivered to the ZedBoard (Xilinx Zynq-7000) that performed the digital to analog conversion after setting the transmission parameters. This signal was amplified and used to directly modulate the optical source, which was a laser diode L658P040 with emission wavelength of 658 nm and nominal emission power of 40 mW. The LDM9T laser mount was used to modulate the laser and to set the operation bias current using the LDC250 Laser diode controller. The optical signal at the output of the laser was transmitted through a 75-meter long 1-mm core PMMA GI-POF (OM-Giga from Optimedia) with 0.23 numerical aperture and a measured attenuation coefficient at 658 nm of 0.218 dB/m. At the output of the fiber, the SPD-2-650 integrated receiver (1.2-GHz nominal 3-dB bandwidth and conversion factor of 500 mV/mW measured with the OM-Giga at 658 nm) converted the optical signal back to the electrical domain. This signal was then fed back to the electronic board, digitized and stored in the computer in order to get demodulated and analyzed. Simultaneously, power spectral density and total power of the received signal were measured with the Spectrum Analyzer (E4404B from Agilent).

In order to configure the link and gain insight of the effect of the active devices and the fiber itself, optical back-to-back measurements were performed. Fig. 2(a) shows the power characteristic curve of the transmitter measured with a 75-cm GI-POF pigtail, where the selected bias current is represented as a bullet. On the other hand, measurements of the S_{21} scattering parameter of the back-to-back system were conducted using a

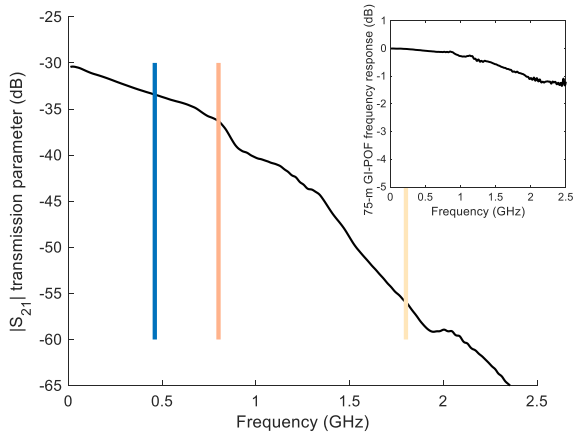

Fig. 3. Frequency response of the transmission system indicating the attenuation expected at the different carrier frequencies considered. The inset shows the normalized frequency response of the 75-meter GI-POF.

Vector Network Analyzer. Fig. 2(b) shows the results obtained for different laser bias currents.

As the graphs show, the transmitter exhibits a quasi-linear input-output characteristic curve above the threshold current, which was measured to be 32 mA. Regarding the system back-to-back frequency response, very noticeable differences are observed below 60-mA bias current, while only small degradations are found above this level. According to these results, we chose to operate the laser at a bias current of 75 mA, which is quite centered within its linear operation range and represents a trade-off between bandwidth degradation and optical power budget.

The complete link frequency response was obtained including the 75-meter fiber segment by measuring the S_{21} parameter from the RF laser input to the optical receiver output. The S_{21} magnitude is represented in Fig. 3 showing that the system has a 3-dB bandwidth of 800 MHz and a gain or attenuation that differs for the different carrier frequencies being -33.45 dB for the transmission over a carrier frequency of 460 MHz, -36.33 dB for 800 MHz and -55.96 dB for the transmission over 1800 MHz. Also, we have included as an inset the frequency response of the fiber, which was obtained by eliminating the effect of the active devices that were estimated from the back-to-back measurement.

As can be observed from the graphs, the fiber has a very flat frequency response, consistent with a reduced dispersion due to its index profile. Therefore, we can conclude that the main components that are responsible for the roll-off in the system frequency response are the active devices. In fact, considering the 3-dB bandwidth of the receiver, we can state that the major bandwidth limiting factor in our set-up is the transmitter.

B. Transmission Parameters

The LTE carrier frequencies considered in the study were 460 MHz, 800 MHz and 1800 MHz. According to the LTE standard, at 460-MHz carrier frequency the only possible LTE bandwidth was 5 MHz. For the higher frequencies 5, 10, 15 and 20 MHz were used. The introduction of IoT services in this signal was done by using the LTE guardband and Narrow-Band IoT for a spectrally efficient transmission. For the different LTE signals, it was possible to allocate the NB-IoT signal in a set of LTE Physical Resource Blocks (PRB). In the analysis, we considered the transmission of NB-IoT signals only in the two PRBs at the high frequency end, since they are likely to be suffer more attenuation than their low-frequency counterparts. When there were several possible PRBs, we chose the closest and the farthest to the LTE signal. The specific values are shown in Table I.

TABLE I
RF TRANSMISSION PARAMETERS

Carrier Frequency (MHz)	LTE Bandwidth (MHz)	Signal RF Power (dBm)	In-band PRBs	Guardband PRBs	PRB used for NB-IoT
460	5	-17.9 – 4.3	0 – 24	-1, 25	25
800	5	-15.9 – 6.4	0 – 24	-1, 25	25
	10	-16.0 – 5.9	0 – 49	-2, -1, 50, 51	50 / 51
	15	-16.0 – 5.9	0 – 74	-4 – -1, 75 – 78	75 / 78
	20	-16.4 – 5.5	0 – 99	-5 – -1, 100 – 104	100 / 104
1800	5	-12.2 – 9.7	0 – 24	-1, 25	25
	10	-11.6 – 10.1	0 – 49	-2, -1, 50, 51	50 / 51
	15	-11.6 – 10.1	0 – 74	-4 – -1, 75 – 78	75 / 78
	20	-12.2 – 9.5	0 – 99	-5 – -1, 100 – 104	100 / 104

The RF input power used to modulate the laser source was a key parameter of this analysis. Its value was varied over a 22-dB range whose initial value depended on the carrier and bandwidth according to the data included in Table I. We also considered as a variable parameter the relative power level between the LTE signal and the NB-IoT signal. This parameter, called in the following NB-IoT power boost, was varied in the range from -6 to $+6$ dB in order to analyze its effect over the transmission quality of both the LTE and the NB-IoT signals.

III. RESULTS

In order to obtain the transmission performance of both the LTE and the NB-IoT signal, we estimate the EVM at the receiver end. In this section, we present the results obtained for a selected set of conditions to illustrate how the system performance is affected by the different transmission parameters (RF input power, boost, LTE bandwidth, etc.) Also, Power Spectral Density of the received combined signal is presented here in order to provide a deeper insight of the system behavior. Finally, we summarize the system performance in terms of minimum EVM, and range of input RF powers where the EVM is below the maximum required by the standard for all carrier frequencies and bandwidths.

A. Error Vector Magnitude (EVM)

For all conditions under test, transmission performance of the RoPOF system was evaluated through the estimation of the average EVM. This parameter was obtained both for the downlink LTE and NB-IoT signals once the demodulation was performed at the computer. For every carrier frequency and bandwidth from Table I, EVM results were obtained as a function of input RF power and NB-IoT power boost, which leads to EVM

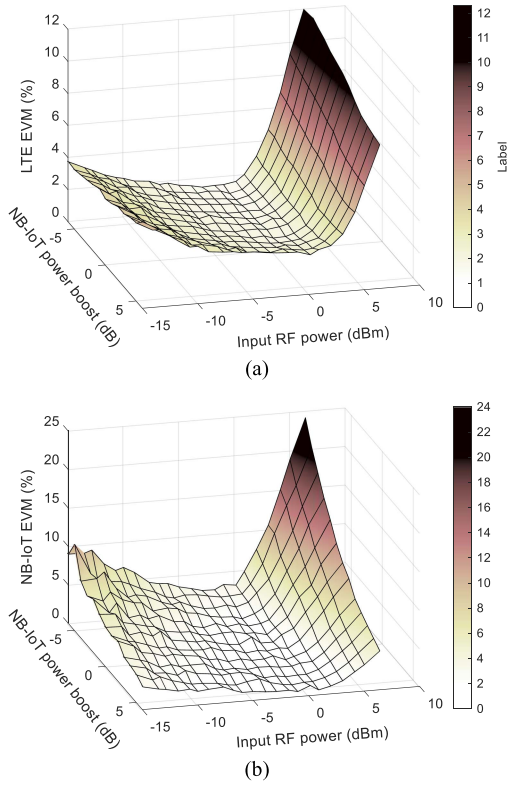

Fig. 4. Average EVM as a function of NB-IoT power boost and input RF power for the LTE signal (a) and the NB-IoT signal (b).

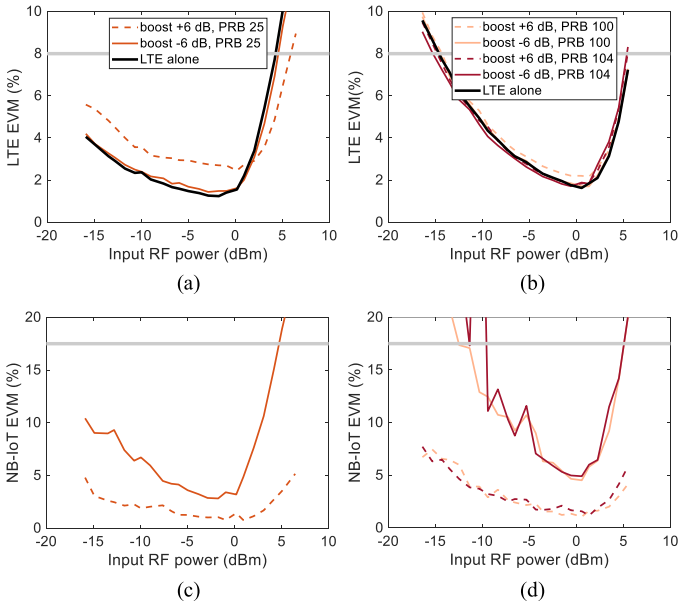

Fig. 5. LTE EVM (a), (b) and NB-IoT EVM (c), (d) as a function of input RF power for +6-dB and -6-dB NB-IoT power boost in the case of 800-MHz carrier frequency and LTE bandwidths of 5 MHz (a), (c) and 20 MHz (b), (d).

surfaces or 3-D plots. As an example, the EVM for the carrier frequency of 800 MHz with a 5-MHz bandwidth is shown for the LTE signal and for the NB-IoT signal in Fig. 4, in the upper and lower graphs respectively. For the 5-MHz LTE bandwidth the NB-IoT transmission is always carried out using the PRB 25.

The EVM 3-D plots in Fig. 4 show a similar shape for both the LTE and NB-IoT signals, increasing at the lower and higher values of input RF power. EVM degradation at the lower input power values can be explained by the lower Signal-to-Noise Ratio (SNR) at the receiver while the EVM rise at higher input power values can be related to a non-linear behavior that distorts the signal. Fig. 4 also shows that the presence of the NB-IoT signal has little effect on the transmission of the LTE signal, which is demonstrated by the small change in the LTE signal EVM when increasing the NB-IoT power boost. On the other hand, the NB-IoT EVM steeply decreases with increasing boost as should be expected. For most of the tested parameter values, the obtained EVMs are below the maximum values established by the standard, which is 8% for the LTE signal and 17.5% for the NB-IoT signal.

In order to evaluate the effect of LTE signal bandwidth and Physical Resource Block (PRB) position, the EVM curves obtained for the carrier frequency of 800 MHz for different conditions are shown in Fig. 5. The EVM for the LTE signal is shown in the upper graphs and for the NB-IoT in the lower graphs. The results for the LTE narrowest and widest bandwidths are shown: on the left graphs for 5 MHz, and on the right graphs, for 20 MHz. In each graph, the EVM curves for the extreme boost values (+6 dB and -6 dB) and for the two tested PRBs (closest and farthest to the LTE signal) are plotted.

Additionally, the EVM obtained when only the LTE signal is transmitted is also shown in the upper graphs to assess the effect of adding the guardband NB-IoT signal. The horizontal lines show the maximum admissible EVM values for the LTE and NB-IoT signals according to the standard. These measurements confirm that the transmission of the NB-IoT signal has little effect on the EVM of the LTE signal, independently of the LTE bandwidth. In fact, EVM shows only a small penalty for the maximum tested boost of +6 dB and the closest PRBs (25 and 100, respectively) as the dotted blue lines show. On the other hand, the boost has a considerable impact on the transmission of the NB-IoT, whose minimum EVM significantly increases when decreasing power boost.

In addition, Fig. 5 shows that increasing the LTE bandwidth shifts the EVM curves for both signals upwards and rightwards. This effect is more noticeable for the NB-IoT signal with the lowest power boost. Thus, the upward shift points out that an increase of the LTE bandwidth produces a slight rise of EVM. The rightward shift indicates that, for wider bandwidths, more input power is necessary to reach the minimum EVM values. These effects will be quantified in Section II-C. Moreover, the degradation of EVM for lower RF input power is steeper for the 20-MHz LTE bandwidth. The position of the PRBs, however, has little effect over the EVM for both signals. Therefore, in the following we will show an average of the EVM measured for the two PRBs considered for each case of LTE bandwidth.

Fig. 6 shows the EVM as a function of signal RF power for all carrier frequencies and bandwidths for LTE (upper graph)

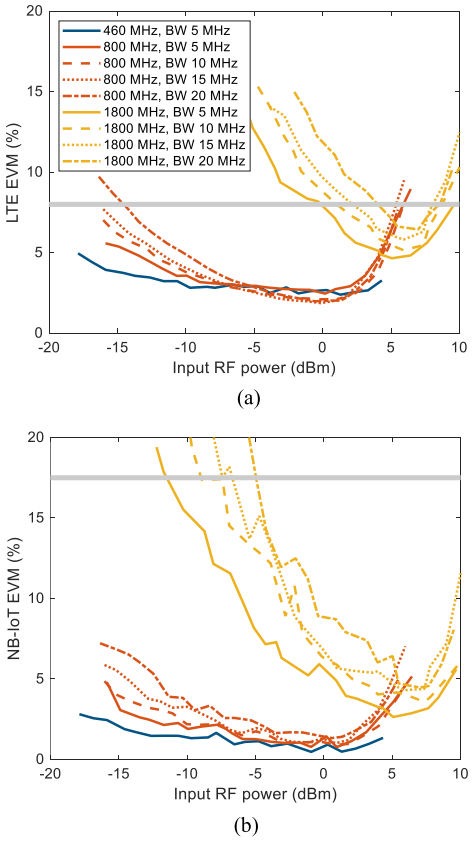

Fig. 6. LTE EVM (a) and NB-IoT EVM (b) as a function of input RF power for +6-dB NB-IoT power boost and the whole set of frequency carriers and bandwidths.

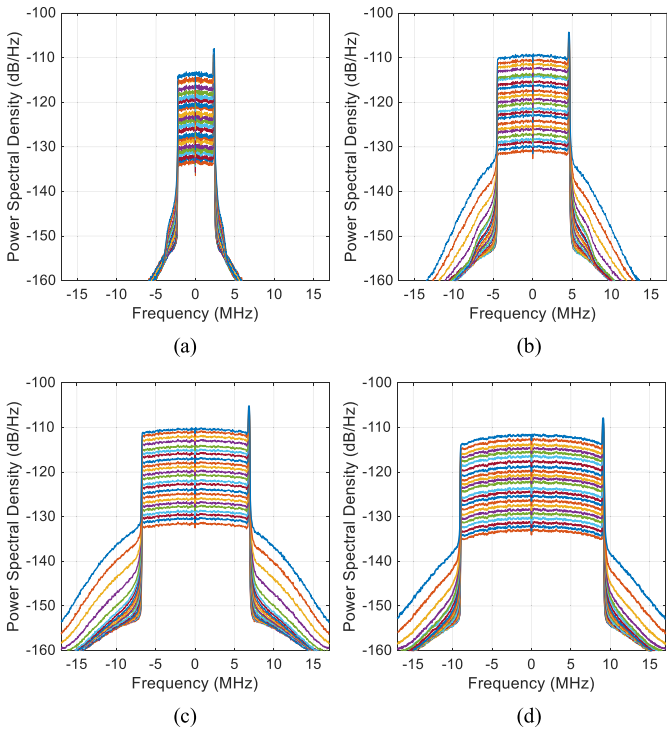

Fig. 7. Power spectral density of the received signal for the different input RF powers considered in the case of 800-MHz carrier frequency and LTE bandwidths of 5 MHz (a), 10 MHz (b), 15 MHz (c) and 20 MHz (d).

and NB-IoT (lower graph). Despite the fact that the whole set of EVM measurements has been obtained, only the EVM for the case +6 dB boost is shown since this power boost gives the best EVM values for the NB-IoT signal and has little effect over the LTE signal. Results show that for a given carrier frequency, the differences of EVM for different bandwidths are greater at lower input RF powers, with higher error for the wider bandwidths. This effect is observed in both signals and can be attributed to the fact that at lower input RF powers the limited SNR is the main factor affecting EVM degradation, and SNR decreases as the signal bandwidth increases.

The effect of increasing the carrier frequency is similar to those visualized when increasing LTE bandwidth at the same carrier frequency. It produces a shift of the EVM curves towards higher input RF powers and towards higher EVM values for both signals. In fact, although the difference between the curve for 460 MHz and the curves for 800 MHz is small, the EVM values for 1800 MHz are much higher for most of the input RF power range. Nonetheless, there is always a range of input powers for which the EVM is below threshold for both the LTE and the NB-IoT signals, although it is much narrower for 1800 MHz. We argue that the transmission performance is degraded at 1800 MHz relative to the other carrier frequencies because of the system frequency roll-off shown in Fig. 3. In fact, at this frequency the signal to noise ratio is reduced by 20 dB.

B. *Power Spectral Density*

In Fig. 7, we represent the measured power spectral density (PSD) of the combined signals (LTE and NB-IoT) at the output of the system for the carrier frequency of 800 MHz, a power boost of 6 dB and the PRB closest to the LTE band. The graphs show the results for the four possible LTE bandwidths. (5, 10, 15 and 20 MHz) and each of the 23 values of input RF power in 1-dB step considered (see Table I), which are shown in different colors. The PSDs show how the LTE and NB-IoT signals are combined for simultaneous transmission: the LTE signal at the center of the carrier frequency (considered as reference of the horizontal axis) and the 180-kHz bandwidth NB-IoT signal in the higher frequency guardband. Also, the power spectra reveal the presence of spectral regrowth at both sides of the LTE channel or main channel that increases dramatically as the input RF power increases. Power leakage to the adjacent channels can be attributed to the presence of non-linear distortion introduced by the active devices and it is the cause of the EVM rise at high RF power values. In fact, the LTE signals are transmitted using Orthogonal Frequency Division Multiplexing (OFDM), making them prone to non-linear distortion due to the high PAPR (Peak to Average Power Ratio). In our case, the value of PAPR was 11.18 dB, which is a typical value for this transmission technique [33].

C. *Summary of Results*

To assess the applicability of our proposal, we have extracted several parameters from our measurements: minimum EVM, RF

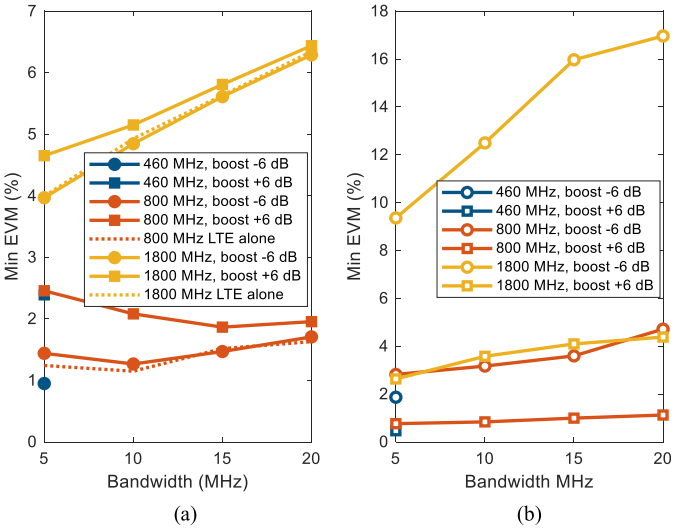

Fig. 8. Minimum EVM for the LTE signal (a) and the NB-IoT signal (b) as a function of LTE bandwidth for the three carrier frequencies and −6 and +6-dB boosts.

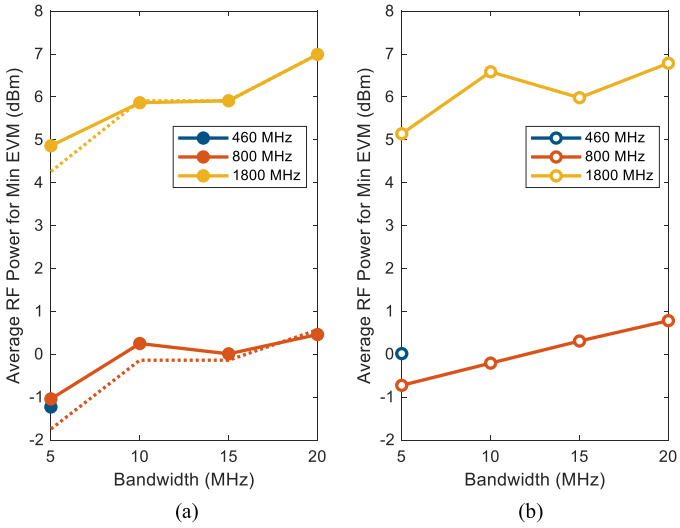

Fig. 9. Input RF power at which the Minimum EVM is reached for the LTE signal (a) and the NB-IoT signal (b) as a function of LTE bandwidth for the three carrier frequencies.

input-power at which the minimum EVM is reached, and range of input RF powers for which the EVM is below the standard threshold.

First, Fig. 8(a) and (b) show the minimum achievable EVM as a function of LTE bandwidth for all carrier frequencies and the LTE and NB-IoT signals, respectively. Carrier frequencies are shown in different colors in both graphs, whereas the different symbols show the +6dB and −6dB boosts, respectively. In Fig. 8(a) the EVM values when the LTE signal is transmitted alone are also shown as dotted lines. As can be observed, the most critical parameter affecting EVM is the carrier frequency due to the shape of the frequency response of the system as discussed before. Increasing LTE bandwidth tends to increase the EVM of the NB-IoT signal, but this effect is small except for the highest carrier frequency. For this frequency, the EVM of the LTE signal also increases with increasing bandwidth. Power boost has a high impact on the NB-IoT EVM, particularly for 1800 MHz, but for the LTE EVM this rise is moderate and tends to be reduced for higher LTE bandwidths. Notice that the EVM for LTE alone is practically equal to the EVM for a −6 dB boost. It is important to point out that the NB-IoT signal can be transmitted with a very small EVM even at the highest carrier frequency of 1800 MHz because of its narrow bandwidth (180 kHz) if the power boost is sufficiently high.

Fig. 9(a) and (b) show the input RF power values at which the minimum EVM is reached as a function of bandwidth for the LTE signal and the NB-IoT signal, respectively. The results obtained for all tested boost and PRB position values have been averaged. The plots show that the power needed to get the minimum EVM has similar values and behavior for both signals, with a slight increase with LTE bandwidth. Furthermore, the required power at 1800 MHz is significantly higher (about 6 dB) than for the other two carrier frequencies, for which it is always below 1 dBm.

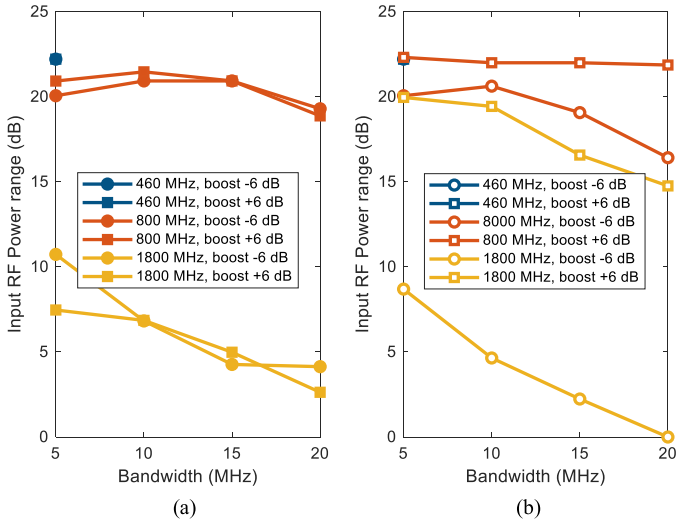

Fig. 10. Range of input RF power for which the EVM is below the standard threshold for the LTE signal (a) and the NB-IoT signal (b) as a function of LTE bandwidth for the three carrier frequencies.

As for the range of RF input powers for which the EVM is below the standard quality threshold, Fig. 10(a) and (b) show that there is a wide range of power with feasible simultaneous transmission. For carrier frequencies of 460 MHz and 800 MHz this range is above 15 dB for both signals and power boosts. In contrast, the range is reduced for the LTE signal and for the NB-IoT signal with a −6 dB boost at 1800 MHz. In these cases, the range also decreases more sharply with increasing LTE bandwidth. For a +6 dB power boost, the feasible input RF power range for succesful NB-IoT transmission is equal or greater than for the LTE signal at the same carrier and bandwidth. In fact, for the NB-IoT signal the power range at 1800 MHz obtained with a +6 dB power boost is only slightly below those found for the other carrier frequencies.

In summary, our results demonstrate the feasibility of transmitting LTE and guardband NB-IoT at 460 MHz, 800 MHz and 1800 MHz for a wide range of input RF powers. There are two main factors that limit the performance, increasing the EVM and reducing the range of suitable RF powers. On the one hand, the frequency response of the optoelectronic devices in the system limits the minimum usable signal power and could be improved by optimizing the design of the laser driver and receiver electronics. On the other hand, the non-linear behavior that appears at the higher RF power values, could be mitigated by different techniques [10], [34]. Moreover, this would reduce the out-of-band power leakage enabling the transmission of several LTE channels and enabling a high throughput RoPOF link.

IV. Conclusion

In this work we have analyzed the transmission of Cellular NB-IoT waveforms for short-distance communications such as those found in automotive, domestic and industrial environments using large-core PMMA Plastic Optical Fibers (POFs). We have demonstrated that it is possible to transmit combined LTE and NB-IoT signals through a 75-meter PMMA graded-index POF with low EVM values for a wide range of relatively low input RF powers, fulfilling the requirements of guardband transmission mode required in 3GPP specifications. Results show that the 6 dB power boost constrain is important to achieve a good performance according to our analysis of the impact of this parameter in a RoPOF link. Furthermore, our study reveals that the frequency band used for transmission is strongly limited by the bandwidth characteristics of the link, which are determined to a large extent by the optoelectronic components for large-core POFs. Nevertheless the successful RoPOF transmission through a 75-meter fiber link paves the way for the use of plastic optical fibers in future hybrid fiber-wireless networks with added IoT capability.

References

[1] C. Lim, Y. Tian, C. Ranaweera, T. A. Nirmalathas, E. Wong, and K.-L. Lee, "Evolution of radio-over-fiber technology," *J. Lightw. Technol.*, vol. 37, no. 6, pp. 1647–1656, Mar. 2019.

[2] C. Lim and A. Nirmalathas, "Radio-over-fiber technology: Present and future," *J. Lightw. Technol.*, vol. 39, no. 4, pp. 881–888, Feb. 2021.

[3] I. B. F. de Almeida, L. L. Mendes, J. J. P. C. Rodrigues, and M. A. A. da Cruz, "5G waveforms for IoT applications," *IEEE Commun. Surveys Tut.*, vol. 21, no. 3, pp. 2554–2567, thirdquarter 2019.

[4] "Evolved universal terrestrial radio access (E-UTRA); physical channels and modulation," document TS-36.211 V17.3.0, 3GPP, Release Mar. 17, 2023.

[5] M. Kanj, V. Savaux, and M. Le Guen, "A tutorial on NB-IoT physical layer design," *IEEE Commun. Surveys Tut.*, vol. 22, no. 4, pp. 2408–2446, Fourthquarter 2020.

[6] G. Pandey, A. Choudhary, and A. Dixit, "Wavelength division multiplexed radio over fiber links for 5G fronthaul networks," *IEEE J. Sel. Areas Commun.*, vol. 39, no. 9, pp. 2789–2803, Sep. 2021.

[7] J. S. Wey and J. Zhang, "Passive optical networks for 5G evolution," *Proc. SPIE*, vol. 10559, Jan. 2018, Art. no. 105590N.

[8] C. Vazquez et al., "Multimode fibers in millimeter-wave evolution for 5G cellular networks," *Proc. SPIE*, vol. 9772, Feb. 2016, Art. no. 97720F.

[9] A. Raza, S. Ghafoor, and M. F. U. Butt, "MIMO-enabled integrated MGDM–WDM distributed antenna system architecture based on plastic optical fibers for millimeter-wave communication," *Photon. Netw. Commun.*, vol. 35, no. 2, pp. 265–273, 2018.

[10] T. Aiba et al., "28 GHz band 5G mobile radio signal transmission employing graded-index plastic optical fibers," in *Proc. 28th Int. Conf. Plast. Opt. Fibers*, 2019, pp. 43–44, Paper 3 01.

[11] A. Inoue and Y. Koike, "Low-noise radio over graded-index plastic optical fiber," *Opt. Lett.*, vol. 45, no. 12, pp. 3192–3195, Jun. 2020.

[12] K. Muramoto, A. Inoue, and Y. Koike, "Noise and distortion reduction in OFDM radio-over-fiber link by graded-index plastic optical fiber," *IEEE Photon. Technol. Lett.*, vol. 32, no. 13, pp. 835–838, Jul. 2020.

[13] D. Zaremba and R. Evert, "Materials, chemical properties and analysis," in *Polymer Optical Fibres Fibre Types, Materials, Fabrication, Characterisation and Applications*, 1st ed., C. A. Bunge, T. Gries, and M. Beckers, Eds. Amsterdam, The Netherlands: Elsevier, 2017, ch. 5, pp. 153–186.

[14] K. Koike and Y. Koike, "Design of low-loss graded-index plastic optical fiber based on partially fluorinated methacrylate polymer," *J. Lightw. Technol.*, vol. 27, no. 1, pp. 41–46, Jan. 2009.

[15] Y. Koike and K. Koike, "Progress in low-loss and high-bandwidth plastic optical fibers," *J. Polym. Sci. Part B Polym. Phys.*, vol. 49, no. 1, pp. 2–17, Jan. 2011.

[16] S. W. Park, "Production, properties and future of PMMA-GI-POF," in *Proc. 21st Meeting ITG-SC 5.4.1*, 2006.

[17] A. Lopez, N. Villar, A. Losada, E. Laporta, and J. Mateo, "Experimental characterization of the transmission properties of large-core graded-index PMMA fibers," in *Proc. IEEE 22st Int. Conf. Transparent Opt. Netw.*, 2020, pp. 1–5.

[18] A. Grzemba, *MOST: The Automotive Multimedia Network*. Haar, Germany: Francis Verlag, 2011.

[19] SERCOS I/II, 2022. [Online]. Available: https://www.sercos.org/technology/sercos-i-and-ii

[20] Y.-K. Lee and D. Lee, "Broadband access in Korea: Experience and future perspective," *IEEE Commun. Mag.*, vol. 41, no. 12, pp. 30–36, Dec. 2003.

[21] Y. Koike, "Status of high-speed plastic optical fibre towards giga house town," in *Proc. 18th Int. Conf. Plast. Opt. Fibers*, 2009, pp. 1–5, Paper P21.

[22] A. Nespola et al., "In-building and home networks using POF," in *Proc. IEEE LEOS Annu. Meeting Conf.*, 2009, pp. 624–625.

[23] G. Stepniak, G. M. Schuppert, and C. A. Bunge, "Polymer-optical fibres for data transmission," in *Polymer Optical Fibres Fibre Types, Materials, Fabrication, Characterisation and Applications*, 1st ed. C. A. Bunge, T. Gries, and M. Beckers, Eds. Amsterdam, The Netherlands: Elsevier, 2017, ch. 8, pp. 218–310.

[24] KDPOF. Accessed: Nov. 10, 2023. [Online]. Available: https://www.kdpof.com/home-soho/

[25] J. M. B. Oliveira, S. Silva, L. M. Pessoa, D. Coelho, H. M. Salgado, and J. C. S. Castro, "UWB radio over perfluorinated GI-POF for low-cost in-building networks," in *Proc. IEEE Int. Topical Meeting Microw. Photon.*, 2010, pp. 317–320.

[26] D. Visani et al., "Wired and wireless multi-service transmission over 1mm-core GI-POF for in-home networks," *Electron. Lett.*, vol. 47, no. 3, pp. 203–205, 2011.

[27] M. Beltrán et al., "DVB-S2 and DVB-T RF transmission in 1-mm GIPOF system," *IEEE Photon. Technol. Lett.*, vol. 26, no. 16, pp. 1665–1668, Aug. 2014.

[28] F. Forni, Y. Shi, N. C. Tran, H. P. A. van den Boom, E. Tangdiongga, and A. M. J. Koonen, "Multiformat wired and wireless signals over large-core plastic fibers for in-home network," *J. Lightw. Technol.*, vol. 36, no. 16, pp. 3444–3452, Aug. 2018.

[29] Z. Shouran, A. Ashari, and T. Priyambodo, "Internet of Things (IoT) of smart home: Privacy and security," *Int. J. Comput. Appl.*, vol. 182, no. 39, pp. 3–8, 2019.

[30] D. Elliott, W. Keen, and L. Miao, "Recent advances in connected and automated vehicles," *J. Traffic Transp. Eng. (English Ed.)*, vol. 6, pp. 109–131, 2019.

[31] W. Z. Khan, M. H. Rehman, H. M. Zangoti, M. K. Afzal, N. Armi, and K. Salah, "Industrial Internet of Things: Recent advances, enabling technologies and open challenges," *Comput. Elect. Eng.*, vol. 81, 2020, Art. no. 106522.

[32] M. Waseem, A. López, P. L. Carro, and M. A. Losada, "Radio over plastic optical fiber transmission for short-range future networks," in *Proc. Glob. Conf. Wireless Opt. Technol.*, 2022, pp. 1–4.

[33] C. Mateo, P. L. Carro, P. Garcia-Ducar, J. de Mingo, and I. Salinas, "Evaluation of nonlinear effects in a RoF SpatialMux MIMO-LTE fronthaul system," in *Proc. IEEE 87th Veh. Technol. Conf.*, 2018, pp. 1–5.

[34] M. U. Hadi et al., "Linearity improvement of VCSELs based radio over fiber systems utilizing digital predistortion," *Adv. Sci. Technol. Eng. Syst. J.*, vol. 4, no. 3, pp. 156–163, 2019.